

A World-Wide Ionospheric Model for Fast Precise Point Positioning

A. Rovira-Garcia, J. M. Juan, J. Sanz, G. González-Casado

Abstract—Fast Precise Point Positioning (Fast-PPP) is a satellite-based navigation technique using an accurate real-time ionospheric modeling to achieve high-accuracy quickly. In this work, an end-to-end performance assessment of Fast-PPP is presented in near-maximum Solar Cycle conditions; from the accuracy of the Central Processing Facility corrections, to the user positioning. A planetary distribution of permanent receivers including challenging conditions at equatorial latitudes, is navigated in pure kinematic mode, located from 100 to 1300 kilometers away from the nearest reference station used to derive the ionospheric model. It is shown that satellite orbits and clocks accurate to few centimeters and few tenths of nanoseconds, used in conjunction with an ionosphere with an accuracy better than 1 Total Electron Content Unit (16 centimeters in L1) reduce the convergence time of dual-frequency Precise Point Positioning, to decimeter-level (3D) solutions. Horizontal convergence times are shortened 40% to 90%, while the vertical components are reduced by 20% to 60%. A metric to evaluate the quality of any ionospheric model for Global Navigation Satellite System is also proposed. The ionospheric modeling accuracy is directly translated to mass-market single-frequency users. The 95th percentile of horizontal and vertical accuracies are shown to be 40 and 60 centimeters for single-frequency users and 9 and 16 centimeters for dual-frequency users. The trade-off between the formal and actual positioning errors has been carefully studied to set realistic confidence levels to the corrections.

Index Terms—Global Navigation Satellite System (GNSS), Precise Point Positioning (PPP), real-time ionospheric corrections, undifferenced ambiguity fixing.

I. INTRODUCTION

TWO state-of-the art high-precision positioning services (HPPS) offer positioning accuracy at the centimeter level: Real-Time Kinematics (RTK) and PPP. Both rely on carrier-phase measurements, typically two orders of magnitude more precise than codes, but they contain the carrier-phase ambiguity as an additional unknown. Classical (two-receiver baseline) RTK [1] uses the time-tagged measurements of all satellites in view at a close reference receiver to compensate for most of the delays affecting the GNSS signals. Thence, the relative baseline vector to a reference station is estimated to centimeter-level accuracy, in some tens of seconds.

Precise relative positioning is limited by the spatial error decorrelation. Even with a benign ionosphere, the assumption

of a differential ionospheric delay being either negligible between the rover and the reference receiver is not valid for baselines greater than a few tens of kilometers. Baselines are enlarged using the network atmospheric modeling of the Network RTK (NRTK) [2] approach. However, a large number of base stations would be needed to provide a planetary service. Moreover, if measurements were broadcast using the Radio Technical Commission for Maritime Services (RTCM) format [3], unaffordable bandwidth would be required.

PPP [4] is a high-accuracy technique in undifferenced mode for dual-frequency users with typical accuracies in the order of a decimeter (in kinematic mode) or centimeter (in static mode). It is based on using satellite orbits and clocks significantly more accurate than those broadcast by the GNSS satellites. They are calculated using data from a permanent receiver network, e.g., the International GNSS Service (IGS) [5], and an accurate modeling of the measurements down to the centimeter level. Since orbits and clocks are satellite-dependent, global coverage is achieved with limited bandwidth. A review of current commercial PPP services can be found in [6].

In PPP, the ionospheric delay is removed (up to 99.9% [7]) thanks to the dual-frequency ionospheric-free combination. However, the Classical PPP requires more time to achieve high-accuracy navigation than RTK [8], since the ambiguities are estimated as real numbers (i.e., floated ambiguities), instead of fixed integers as in relative positioning. Indeed, sufficient change must be observed in satellite geometry to decorrelate (separate) floated ambiguities from the other parameters being estimated in the navigation filter. The main drawback of PPP is this convergence, which depends on satellite geometry. Generally, it takes the best part of one hour with Global Positioning System (GPS), although the process is shorter in full multi-constellation environments.

The further developments presented in [9]–[12] added to PPP the capability of undifferenced ambiguity fixing. The convergence time drawback of PPP was tackled in [13], thanks to an accurate regional ionospheric modeling based on GNSS data. This last technique, known as Fast Precise Point Positioning (Fast-PPP), was invented by the Research group of Astronomy and Geomatics (gAGE/UPC). It is protected by several international patents [14] funded by the European Space Agency (ESA), including also the use of triple-frequency signals [13].

In this work, Fast-PPP is extended to a planetary scale. We test how permanent receivers, treated as rovers, reduce the convergence time of their navigation solution (improving the accuracy since any cold start). The Fast-PPP enhancement is assessed against current ionosphere-free solutions; not only for dual-frequency receivers that can use the aforementioned

Manuscript received XXX XX, XXXX; revised xxxxx xx, xxxx.

A. Rovira-Garcia, J. M. Juan, J. Sanz and G. González-Casado are with the Research Group of Astronomy and GEomatics (gAGE/UPC), 08034 Barcelona, Spain (e-mail: {adria.rovira, jose.miguel.juan, jaume.sanz, guillermo.gonzalez}@upc.edu).

This work has been partially sponsored by the ESA Network Partner Initiative with the industrial partner FUGRO. The Technical University of Catalonia contributed with a FPI-UPC grant. Projects GNAVIS from EC-FP7 and ANTARTIDA CTM2010-21312 have also supported this work.

Digital Object Identifier xx.xxxx/TGRS.xxxx.xx

TABLE I
OVERVIEW OF FAST-PPP CPF CORRECTIONS

Correction	Update time	Content	Service
Fast	5s	Satellite Clocks	Classic PPP
Slow	300s	Satellite Orbits	
		Satellite DCB	Undifferenced
Ionosphere	300s	Fractional part of ambiguities	Ambiguity Fixing
		Unambiguous VTEC grid	Fast-PPP Mass-market

PPP, but also for single-frequency receivers that can use the Group and Phase Ionospheric Calibration (GRAPHIC) technique described in [15].

The structure of this work is the following: in Section II, we describe how the Fast-PPP Central Processing Facility (CPF) is implemented and we list all the products that delivers. The accuracy of the geodetic corrections (satellite orbits and clocks) is assessed in the Section III. The Fast-PPP ionospheric model is tested with a novel scheme in the Section IV. The user strategy to combine all the externally computed corrections with the GNSS measurements is detailed in Section V. Fast-PPP single- and dual- frequency navigation results are assessed in Section VI, in terms of convergence time, accuracy and confidence in the solution. Finally, Section VII summarizes the results.

II. FAST-PPP CPF

The different products listed in Table I are computed in a unique CPF developed by the authors. Three Kalman filters (fast, slow and iono) run in parallel, fed with GNSS data from three different networks of permanent receivers globally distributed, see Fig. 1. The slow filter uses all stations shown in black to estimate slow-varying satellite parameters: the Differential Code Biases (DCBs), the fractional ambiguities and the satellite orbits. The slow filter corrects (i.e., adjusts) the predicted IGS Ultra-Rapid (IGU) orbits [16] with GNSS measurements using the Hill coefficients, following [17]. Thanks to the accurate geodetic modeling, the slow filter is able to fix the carrier-phase ambiguities: this output will be used by the other two filters. The fast filter, uses the data from the blue subset of receivers to estimate the satellite and receiver clocks as white-noise processes on a much shorter update time. Finally, the third (iono) filter uses data from the red network of stations to refine the DCBs and to estimate the parameters of the Fast-PPP ionospheric model, using the strategy later detailed in Section V.

III. FAST-PPP ORBIT AND CLOCK CORRECTIONS ASSESSMENT

The accuracy of the real-time Fast-PPP orbits and clocks is assessed in Fig. 2 with respect to the most accurate determinations from IGS, i.e., the final products. Available approximately with 15 days of latency, IGS final satellite orbits and clock are accurate to 2.5 centimeters and 0.08 nanoseconds [16], respectively.

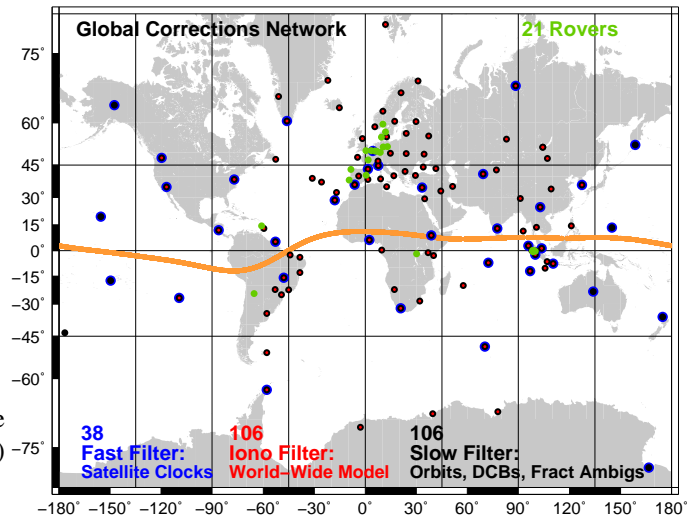


Fig. 1. Distribution of rovers (green) and reference stations (black) along the geomagnetic equator (orange) used to calculate Fast-PPP corrections for the scenario processed on day 150 of Year 2011; satellite clocks (blue), ionospheric corrections (red). All reference stations are used to calculate orbit correction, delay code biases and fractional part of the ambiguities.

The top plot shows the Root Mean Square (RMS) of the difference between the satellite clocks of Fast-PPP (real-time) and the IGS final values. The 24h RMS is 0.22 nanoseconds (~ 6 cm). The bottom plot shows the RMS of the 3D orbit difference of IGS final orbits versus the Fast-PPP real-time estimates (circles) and the predicted IGU orbits (crosses). Fast-PPP orbit error is maintained at 3.9 centimeters, correcting the degradation of IGU until a new orbit set is delivered. This occurs every 6 hours with a typical delay of 3 hours (i.e., the set of orbits predicted at 00^h becomes available at 03^h).

The Fast-PPP orbit and clock accuracies are comparable with the IGS Real-Time Pilot Project (IGS-RTPP) [18] combined product. Indeed, during the experiment (Day of Year (DoY) 150 of Year 2011) the accuracies of the IGS-RTPP were 2.7 centimeters and 0.21 nanoseconds for orbits and clocks respectively, with respect to IGS rapid products. Differences between rapid and final IGS products are negligible [16].

IV. FAST-PPP IONOSPHERIC CORRECTIONS

The convergence time of PPP and GRAPHIC is strongly dependent on the code measurements, which are unambiguous but noisy. This noise slows down the carrier-phase ambiguity estimation process after a user cold start or a cycle slip. The core of Fast-PPP is the capability to calculate real-time ionospheric delays, namely Slant Total Electron Content (STEC) values, with accuracies of around 1 Total Electron Content Unit (TECU). Notice that the nominal accuracy of the Global Ionospheric Maps (GIMs) from IGS is 2-8 TECU in vertical (i.e., not slant) [16].

The accurate Fast-PPP STEC estimates can be used to reduce the transient period of the ambiguity estimation, because i) it is an absolute determination (i.e., undifferenced, unlike other techniques like RTK), ii) unambiguous, and iii) several times more precise than code measurements. The unbiased nature of the Fast-PPP ionosphere leaves untouched the final

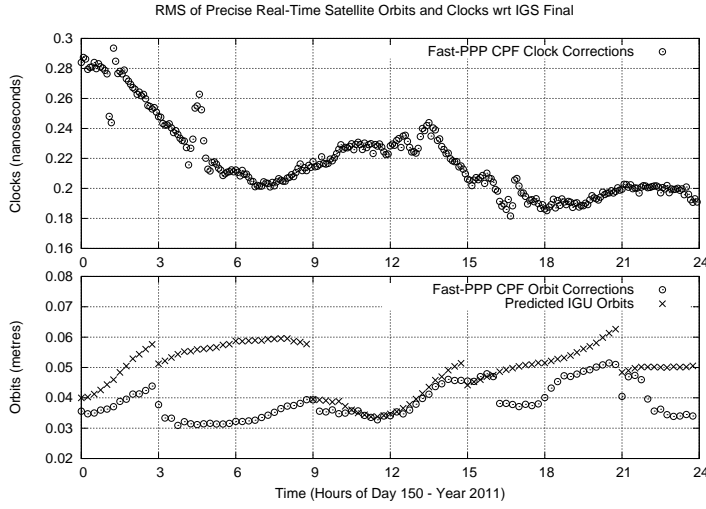


Fig. 2. RMS of real-time Fast-PPP (circles) satellite clock corrections (top, in nanoseconds) and orbit corrections (bottom, in meters). The predicted IGU orbits (bottom, crosses), available in real-time, are corrected by the CPF. In all cases, the difference is calculated with respect to the IGS final products.

accuracy (from the converged filter). The Fast-PPP ionosphere calculation at the CPF is described next.

Besides satellite orbits and clocks, the Fast-PPP CPF also calculates the carrier-phase ambiguities for the frequencies involved (for instance, the GPS L1 and L2 in this work). Once they have been accurately estimated from accurate geodetic modeling, the CPF can fix them to their integer values. In this way, the left hand of (1) is the unambiguous geometry-free ($LI = L1 - L2$ [7]) combination of carrier-phase measurements LI_i^j between the receiver i and the satellite j , once the ambiguity of this combination, BI_i^j , has been corrected. This is the input data for the ionospheric filter, which is very precise, with only the noise of the carrier-phase (i.e., at the level of some millimeters):

$$LI_i^j - BI_i^j = STEC_i^j + DCB_i - DCB^j \quad (1)$$

In this equation, unambiguous carrier-phase measurements can be separated, as in [19], in the ionospheric delay term, $STEC_i^j$, and a constant part: the satellite and receiver DCBs, DCB^j and DCB_i , respectively. Each $STEC_i^j$ is modeled with a lineal combination of the Vertical Total Electron Content (VTEC) delays, $VTEC_k$, on a set of Ionospheric Grid Points (IGPs) every 3 by 3 degrees in two layers (see [20]):

$$STEC_i^j = \sum \alpha_k \cdot VTEC_k \quad (2)$$

Where α_k is a factor which includes the mapping function (i.e., obliquity factor at each layer) and the interpolation from the IGPs to the Ionospheric Pierce Point (IPP). Because α_k depends on the geometry, any change in the ionospheric model geometry (layers height, grid size...) affects to the DCB estimation, when (1) is used.

The use of a two-layer model is motivated by the fact that ionosphere can be separated into two main components: the lower component, or ionosphere and the upper component, or

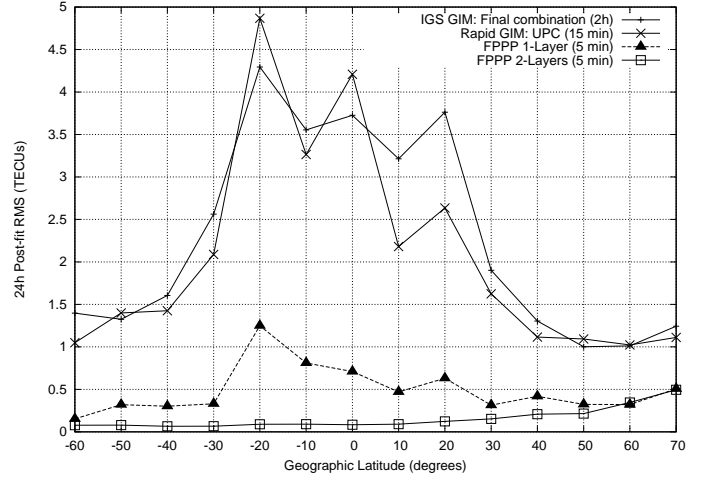
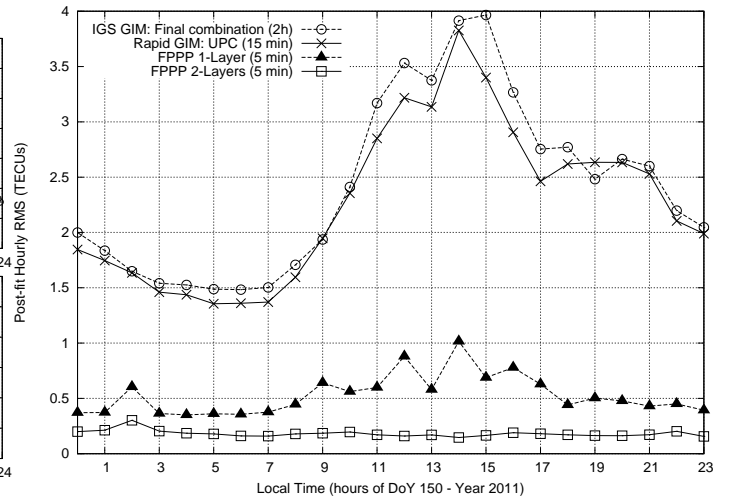


Fig. 3. Results of the consistency test between different ionospheric estimates: 2-hours GIM IGS combined product (circles), 15-minutes GIM UPC product (crosses), and 5-minutes Fast-PPP ionosphere using a single layer (triangles) and two layers (squares). The horizontal axis is local time in the top plot and latitude in the bottom plot.

plasmasphere. Each component has a different height distribution and dynamic evolution, and it is particularly important to consider both in low latitudes.

After a convergence time of several hours (the Fast-PPP CPF starts a day before), the CPF estimates the values and the confidence bounds of the VTECs and the DCBs with typical accuracies of the order of 1 TECU.

A. Fast-PPP ionospheric model assessment

The quality of any ionospheric model for GNSS navigation can be assessed as follows. The left-hand side of (1) can be considered, except for the DCBs, as true ionospheric delays, thanks to the fixed BI . Thence, any ionospheric model $STEC_{model}$ shall differ only from the unambiguous ($LI - BI$), in the hardware delays (i.e., a receiver constant K_i plus a satellite constant K^j):

$$STEC_{model,i}^j - (LI_i^j - BI_i^j) = K_i + K^j \quad (3)$$

The K_i and K^j on the right-hand of the previous equation are estimated by a Least Squares (LS) process. In this way, the post-fit residuals obtained from this adjustment provide a metric to assess the quality of any ionospheric model. Notice that any common bias in $STEC_{model}$ affecting both satellites or receivers will not affect the user navigation solution nor be included in the test results, since it is absorbed into the receiver and satellite constants. In this way, this test is very adequate for assessing ionospheric models tailored for navigation.

In order to have a reference, the test results of the Fast-PPP STECs are compared with the STECs obtained from the well-known IGS GIMs using the standard IONosphere map EXchange format (IONEX) [21]. The residuals from the K^j 's fits in (3) to measurements every 30 seconds, are shown in Fig. 3, using one RMS curve for all reference stations used by the ionospheric filter. The axes local time (top plot) and latitude (bottom plot) most clearly illustrate the differences between models.

On the one hand, the final (post-processed) IGS combined GIMs accuracies, using an update time of 2 hours, are of the order of 1-5 TECUs, which is better than the published accuracies previously mentioned. The estimates of the Technical University of Catalonia (UPC) GIM slightly improve when using a 15-minute sampling rate, indicating that the refresh time is not a key factor, at least, for the scenario considered.

On the other hand, it is shown the accuracy of the Fast-PPP ionospheric model, calculated in real time with a sampling rate of 5 minutes and fixing the ambiguities. It can be seen that the two-layer ionosphere (squares) is the most accurate estimate, clearly better than 1 TECU for all local times and latitudes. The Fast-PPP model using a single-layer grid (triangles) is also included to show that equatorial latitudes cannot be described accurately with this approach, as indicated previously.

From these results, the advantages of using the Fast-PPP method proposed instead of using the IGS GIMs are evident, especially at local times around or after noon and for low latitudes. Indeed, the post-fit residuals are reduced by up to one order of magnitude. This higher accuracy in the ionospheric corrections (1 TECU corresponding to 16.24 centimeters in the L1 band) is directly translated to the user positioning domain with a similar improvement, because orbit and clock accuracies remain well below 10 centimeters.

It should be emphasized that it is important to set realistically the values of the assumptions (standard deviation and process noise) in the ionospheric filter. Greater process noises slightly reduce the post-fit residuals in (3), but the ionospheric corrections lose efficiency in the navigation filter of Fast-PPP users. Indeed, the trade-off between the formal and actual positioning errors depends on the extent to which the confidence level of the corrections is realistic. This relationship has been carefully studied to obtain the positioning results shown in Section VI.

A final remark about the suitability of the proposed ionospheric test should be done. The results account for the minimum error of the ionospheric model being tested, because it uses the reference stations used to compute the model. A second error source comes from the interpolation, when the user interpolates these models to compute the ionospheric

corrections at the actual user IPPs. This interpolation error will degrade the results, depending on the distance from the stations used to derive the ionospheric model, and any ionospheric perturbation deviating from the linearity assumed (e.g., Travelling Ionospheric Disturbances (TIDs), scintillation...).

V. FAST-PPP USER STRATEGY

User strategies are traditionally conditioned by receiver capabilities (i.e., number of frequencies and type of observables). Mass-market single-frequency code receivers rely on ionospheric models such as Klobuchar [22] or NeQuick [23]. Nevertheless, subtracting the modeled delay from the measurements involves a degree of mis-modeling, an uncertainty that is not usually accounted for in the covariance matrix of the navigation filter. Code and phase single-frequency receivers can benefit from the GRAPHIC [15] combination, free of ionospheric mis-modeling since this error term is removed. However, accuracy and convergence are affected due to the estimation of coordinates from a combination with half of the noise code but containing the ambiguities. Finally, dual-frequency code and carrier-phase receivers typically use PPP.

The Fast-PPP navigation filter keeps code and carrier-phase measurements separate from externally calculated CPF corrections, included as additional equations. This is similar to the weighted ionospheric approach described in [24], but in absolute (i.e., undifferenced) mode. The classical PPP dual-frequency positioning system is presented in (4)-(7), without combining the code and carrier (L_1, L_2, P_1, P_2) measurements. Additional terms are the ionospheric contribution in terms of Total Electron Content (TEC) and the DCB split into the rover and satellite contributions; DCB_r and DCB^j .

$$P_1^j = \rho^j + c(\delta t - \delta t^j) + m_t^j \Delta ZTD_{wet} + \tilde{\alpha}_1 (STEC^j + DCB_r - DCB^j) + \varepsilon_{P_1}^j \quad (4)$$

$$L_1^j = \rho^j + c(\delta t - \delta t^j) + m_t^j \Delta ZTD_{wet} + B_1^j + \lambda_1 w - \tilde{\alpha}_1 (STEC^j + DCB_r - DCB^j) + \varepsilon_{L_1}^j \quad (5)$$

$$P_2^j = \rho^j + c(\delta t - \delta t^j) + m_t^j \Delta ZTD_{wet} + \tilde{\alpha}_2 (STEC^j + DCB_r - DCB^j) + \varepsilon_{P_2}^j \quad (6)$$

$$L_2^j = \rho^j + c(\delta t - \delta t^j) + m_t^j \Delta ZTD_{wet} + B_2^j + \lambda_2 w - \tilde{\alpha}_2 (STEC^j + DCB_r - DCB^j) + \varepsilon_{L_2}^j \quad (7)$$

where ρ^j is the euclidean distance from the rover to the j th satellite antenna phase centers, and δt and δt^j are respectively the rover and satellite clocks scaled by c the speed of light in vacuum. The tropospheric mapping m_t accounts for the projected zenith-to-slant delay. Tropospheric *a priori* nominals (hydrostatic and wet) are modeled and subtracted from the measurements, a wet residual ΔZTD_{wet} is estimated. A similar approach is used with the relative rotation (wind-up), w , between satellites and the rover: the satellite contribution is modeled and subtracted from the carrier-phase measurements, the remaining part (i.e., the rover orientation) has to be estimated, since its contribution is different for L_1 and L_2 . Frequency ratios are $\tilde{\alpha}_1 = \frac{1}{\gamma-1}$ and $\tilde{\alpha}_2 = \gamma \tilde{\alpha}_1$ with $\gamma = (f_1/f_2)^2$. At each epoch t , with N_s satellites in view and two frequencies,

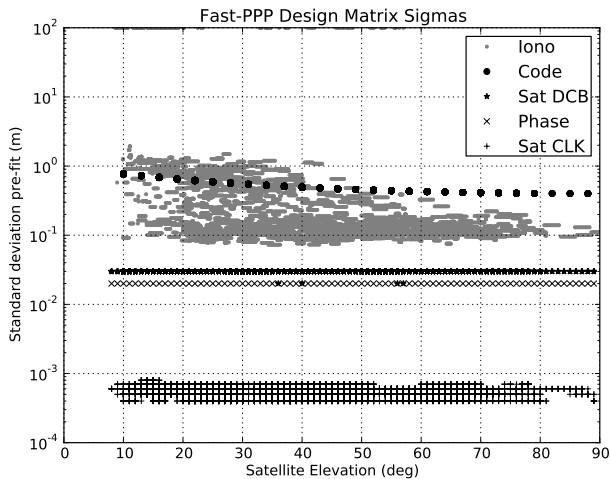


Fig. 4. Example (for rover pbjo) of the standard deviations used in the design matrix to normalize pseudorange (circles) and carrier-phase measurements (crosses), and Fast-PPP corrections: ionosphere (dots), satellite DCBs (stars), and satellite clocks (pluses).

there are $7 * N_s$ equations and $5 * N_s + 7$ unknowns. Single-frequency users only employ (4)-(5). Other constellations are added simply introducing an inter-constellation clock bias unknown and the associated DCB. Fast-PPP corrections: i) satellite clocks, δt_{cor}^j ii) the slant ionospheric delay computed from the two-layer model, $STEC_{cor}^j$ and iii) code biases, DCB_{cor}^j are included by means of:

$$\delta t_{cor}^j = \delta t^j + \varepsilon_{clk}^j \quad (8)$$

$$STEC_{cor}^j = STEC^j + \varepsilon_{ion}^j \quad (9)$$

$$DCB_{cor}^j = DCB^j + \varepsilon_{DCB}^j \quad (10)$$

The ε in each equation accounts for the noise, with a standard deviation σ_ε . This σ_ε is used in the Fast-PPP design matrix to weight the corrections and the GNSS code and carrier-phase measurements as ($W = 1/\sigma_\varepsilon^2$, see Fig. 4). It is assumed that the measurements, (4)-(7), and the corrections, (8)-(10), are uncorrelated. In this way, not only the accuracy of the corrections is relevant, but also the confidence level (sigmas) of the corrections. Corrections are properly bounded by the Fast-PPP CPF, since are key to achieving high-accuracy navigation with adequate confidence limits (formal errors).

The CPF determines the fractional part of the satellite ambiguities for each frequency f_i (and associated λ_i). Their slow change [13] allows its broadcasting as another correction, $\delta B_{i,cor}^j$. The rover part of the fractional ambiguity is canceled by differencing the carrier-phase ambiguities, B_i^j , with respect to a reference satellite, B_i^0 . Thence, integer values of the ambiguities N_i^j are constrained (i.e., fixed) in the navigation filter with the following equation:

$$(B_i^j - \delta B_{i,cor}^j) - (B_i^0 - \delta B_{i,cor}^0) = \lambda_i (N_i^j - N_i^0) \quad (11)$$

There are clear advantages in the Fast-PPP navigation filter strategy of combining the individual measurement, instead of processing their algebraic combinations, as in the classical PPP. First, it is more flexible and high-accuracy navigation is

TABLE II
LOCATION OF ROVERS AND THEIR DISTANCES TO THE NEAREST STATION USED TO CALCULATE THE IONOSPHERIC MODEL

name	coordinates	distance	name	coordinates	distance
unsa	65°W 25°S	1292 km	ebre	00°E 41°N	227 km
nurk	30°E 02°S	761 km	tiku	99°E 00°S	217 km
acor	08°W 43°N	491 km	onsa	12°E 57°N	188 km
vfch	02°E 47°N	415 km	smid	10°E 55°N	185 km
ptbb	10°E 52°N	402 km	eusk	07°E 50°N	170 km
caso	09°W 39°N	376 km	pbjo	99°E 01°S	95 km
klop	09°E 50°N	317 km	lbhu	98°E 00°N	94 km
pots	13°E 52°N	299 km	eijs	06°E 51°N	94 km
osls	10°E 60°N	283 km	dent	03°E 51°N	69 km
hers	00°E 51°N	283 km	ptlo	98°E 00°N	47 km

not interrupted due to a loss of a frequency or measurement, enhancing the robustness of the system in rough environments. Second, the traceability of the protection level calculations is improved by adding each correction with its own sigma. Safe protection levels are obtained even when corrections are degraded, as a result of a poor estimation, network outage, an eclipse or ionospheric events. In this event, great sigmas protect Fast-PPP users, whereas in the classical PPP approach, for instance, satellite clocks are assumed to be error-free.

VI. USER POSITIONING

This section briefly describes how the Fast-PPP navigation has been assessed for DoY 150 of year 2011. The world-wide distribution of permanent receivers, shown as green dots in Fig. 1, has been processed in pure kinematic mode to emulate rovers. Table II shows their coordinates and the distance to the nearest station used to calculate the ionospheric model. Most of the distances range from 100 to 1300 kilometers, more than one order of magnitude greater than typical RTK or NRTK baselines. The rovers used all Fast-PPP corrections: satellite orbits and clocks, the dual-layer ionospheric model together with the DCBs, and the fractional part of the ambiguities.

A. Ionospheric conditions of the assessment

Because the ionospheric corrections are the core of the Fast-PPP technique, it is important to characterize the ionospheric activity during the experiment compared to the conditions in other past assessments, with the same technique, but on a regional scale. In this regard, the hourly VTECs computed from the IGS final GIMs are shown in the top plot of Fig. 5. The VTEC values of the current work (year 2011) at a South-East Asia (SEA) region (crosses) and at a European location (triangles), are shown to be 3 up to 5 times greater than previous Fast-PPP experiments: the strict real-time assessment of 2012 presented in [25] (squares) and the previously mentioned [13] with data of 2009 (circles).

The mean solar radio flux of the day, $112 \times 10^{-22} \text{ W}/(\text{m}^2 \cdot \text{Hz})$, is a medium-to-high value with respect the solar cycle range. In the hourly global geomagnetic Dst index [26] shown in the middle plot of Fig. 5, we can see the recovery period after a geomagnetic storm occurring on DoY 148, but navigation is assessed on a not particularly perturbed day.

An indicator of ionospheric activity that is most sensitive to the regional behavior (and particularly, to the lack of linearity

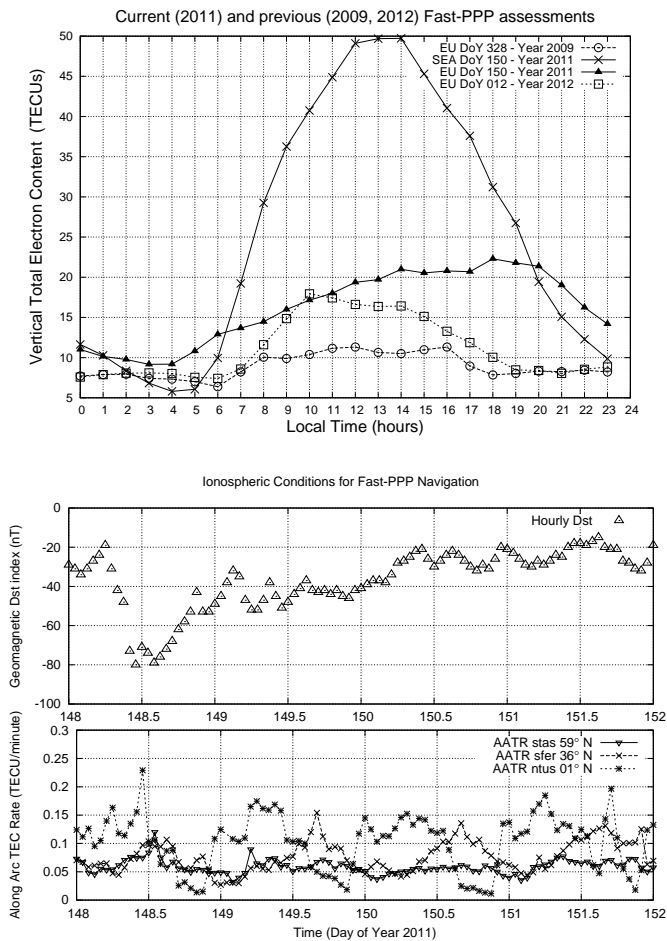


Fig. 5. Top plot: Hourly VTEC for the Equatorial South-East Asian region ($98^{\circ}\text{W}, 0^{\circ}\text{N}$) with respect to a European Mid-latitude ($4^{\circ}\text{E}, 40^{\circ}\text{N}$) for current (DoY 150 of Year 2011) and previous (2009 and 2012) assessments. Middle plot: The global geomagnetic disturbance index Dst . Bottom plot: the ionospheric activity indicator AATR at different reference stations.

of the ionosphere) is the RMS of the Along Arc TEC Rate (AATR) [27]. Moderate values of AATR are shown in the bottom plot for some stations of the ionospheric network, indicating that no scintillation occurred. This is in line with [27], where it was shown that these days of the year (May-June) typically present low scintillation problems. Further studies under ionospheric storms or severe scintillations will be carried out in future works, to prove the role of ionosphere in the rapid phase re-acquisition after massive cycle-slips.

B. Fast-PPP positioning results

Fast-PPP single- and dual-frequency positioning (in kinematic mode) will be shown to reduce the convergence time of the aforementioned ionosphere-free strategies, namely GRAPHIC and classic PPP. In order to assess such improvement, the 24 hours of actual GNSS data collection (with a sampling rate of 30 seconds) are split in 12 intervals of 2 hours. Each 2 hours window is processed independently after applying a full reset to the navigation filter. Then, we can express the navigation error as a function of the time since the last reset for every of the twelve windows. The RMS of such error is computed (i.e., merging the twelve resets) for

the horizontal and vertical components and the associated 3D formal errors.

The impact of the ionospheric modeling in the user domain is assessed by comparing the real-time Fast-PPP ionosphere and a set of corrections from the final combined post-processed IGS GIM. Similar standard deviations in (9) than with Fast-PPP have been used after augmenting the RMS values present in the IGS GIM. This is done in order to optimize the navigation solution when the IGS GIMs are used. Indeed, the more realistic the sigmas are (i.e. properly bounding the ionospheric errors seen in the previous test results), the better the navigation is performed.

Examples of user accuracies together with their 3D formal error are shown in Fig. 6 for single- and dual-frequency navigation modes. The Fast-PPP single-frequency (red) horizontal and vertical performance is remarkable, from the beginning of a cold start with errors of some 30 to 80 centimeters to final converged values of around 20 to 30 centimeters, respectively. Single-frequency Fast-PPP converges several times faster to the GRAPHIC (iono-free) solution plotted in black, while the IGS GIMs (green) present a biased solution, especially for the equatorial rovers. This improvement is at the level of the aforementioned ionospheric test shown in Fig. 3.

While in single-frequency navigation Fast-PPP improves the accuracy, in dual-frequency (pink) it reduces the convergence time needed to achieve a certain level of accuracy, taking into account the confidence (sigma) in the solution, shown in the right row of Fig. 6. In order to quantify the reduction in the convergence time, the following metric is adopted: 1) A threshold for the sigma is set at two times the stationary value of the classical PPP strategy (blue), namely, 15 and 22 centimeters for the horizontal and vertical components respectively. 2) An accuracy threshold is set at three times the final accuracy in each horizontal and vertical component (~ 20 centimeters), since rovers are navigated in kinematic mode. Under these criteria, the Fast-PPP horizontal component reduces the convergence time of PPP the most, with a reduction of 40% to 90%, while the vertical component is reduced by 20% to 60% for the distance range between 100 and 500 kilometers, which can be taken as the maximum distance to the nearest reference station for which ionospheric corrections accelerate the positioning. Moreover, Fast-PPP performance for distances over 800 kilometers or isolated rovers is never worse than the GRAPHIC and PPP solutions, which are taken as the worst-case reference. This is not the case for the IGS GIMs-based single- and dual-frequency navigation shown in green and orange, respectively.

Having shown the improvements in accuracy (single-frequency) and convergence time (dual-frequency), the next factor to assess is the reliability of the positioning, derived from the confidence bounds associated with the corrections. This can be done by means of the Stanford plots, although Fast-PPP is not intended for safety-of-life applications. For this assessment, we have used the 24 hours of data for all rovers in Table II without resetting the user state. Horizontal and vertical 95% accuracies of Fig. 7 are better than 40 and 60 centimeters for single-frequency users and 9 and 16 centimeters for dual-frequency users. Safe margins are

observed for all rovers across the extensive network where several different ionospheric conditions are mixed. Vertical and horizontal protection levels (VPL and HPL) are given as $VPL = 5.33\sigma_V$ and $HPL = 6.00\sigma_H$ following [28].

VII. CONCLUSIONS

An end-to-end performance assessment of the Fast-PPP technique at a planetary scale has been presented. Accuracies of the CPF real-time precise satellite orbits and clocks have been shown to be of the order of IGS real-time products, respectively, a few centimeters and a few tenths of a nanosecond. This enables a global PPP service, enhanced by the Fast-PPP CPF determinations of the fractional part of the ambiguities, to add the capability of global undifferenced ambiguity fixing.

Once that satellite orbits and clocks accurate to some centimeters are made available to users in real time, the limiting factor in high-accuracy positioning is the ionospheric delay. A dedicated metric has been introduced to assess the suitability of ionospheric models for satellite-based navigation. The two-layer, ambiguity-fixed Fast-PPP ionospheric real-time estimates are accurate at the level of 1 TECU (16 centimeters in L1), and can be used in combination with precise orbits and clocks maintaining their accuracy. This is not the case for the IGS GIMs, with accuracies up to one order of magnitude worse. It has been shown, under medium to high solar flux conditions, that the difference between the two ionospheric models is greater at low latitudes and around local noon.

A criterion has been introduced to assess the convergence time based on the accuracy and the confidence level of the solution. Fast-PPP dual-frequency users also benefit from the precise ionospheric modeling through a several-fold reduction in the convergence time compared to the classic PPP solutions, not only in mid-latitude regions but also under more challenging ionospheric conditions such as those found in the equatorial region. This is especially notable for rovers located up to 500 kilometers away from the nearest reference station, which makes feasible the usage of a sparse network. Further or isolated rovers only allow a slight improvement, never worsening the current ionosphere-free solutions, thanks to the realistic confidence levels calculated at the Fast-PPP CPF.

Finally, it has been shown that accuracies of single-frequency users are directly affected by the quality of the ionospheric estimates. Results confirm an improvement in the ionospheric model compared to IGS GIMs, especially at low latitudes. On a planetary scale, Fast-PPP single- and dual-frequency navigation is safely bounded under protection levels of the order of 3.5 and 1.0 meter, respectively.

ACKNOWLEDGMENT

The authors acknowledge the use of data from the International GNSS Service and the Sumatran GPS Array (SuGAR).

REFERENCES

- [1] B. W. Remondi, "Performing centimetre Accuracy Relative Surveys in Seconds Using GPS Carrier Phase," in *First International Symposium on Precise Positioning with the GPS*, Rockville, MD, 1985, pp. 361–377.
- [2] G. Wubbena, A. Bagge, G. Seeber, V. Boder, and P. Hankemeier, "Reducing Distance Dependent Errors for Real Time Precise DGPS Applications by Establishing Reference Station Networks." in *Proceedings of ION GPS 1996*, 1996, pp. 1845–1852.
- [3] RTCM SC-104, "Radio Technical Commission for Maritime Services: Special Committee No.104 Recommended Standards for Differential Navstar GPS Service, Version 2.3, Paper 136-2001/SC104-STD," Alexandria, Virginia, USA, Aug. 2001.
- [4] J. Kouba and P. Héroux, "Precise Point Positioning Using IGS Orbit and Clock Products," *GPS Solutions*, vol. 5, no. 2, pp. 12–28, 2001. [Online]. Available: <http://dx.doi.org/10.1007/PL00012883>
- [5] J. Dow, R. E. Neilan, and C. Rizos, "The International GNSS Service in a changing landscape of Global Navigation Satellite Systems," *Journal of Geodesy*, vol. 83, p. 191198, 2009.
- [6] T. Murfin, "Look, No Base-Station! Precise Point Positioning (PPP)." 2013. [Online]. Available: <http://gpsworld.com/look-no-base-station-precise-point-positioning-ppp>
- [7] J. Sanz, J. Juan, and M. Hernández-Pajares, GNSS Data Processing, Vol. I: Fundamentals and Algorithms. Noordwijk, the Netherlands: ESA Communications, ESTEC TM-23/1, 2013.
- [8] C. Rizos, V. Janssen, C. Roberts, and T. Grinter, "PPP versus DGNSS," *Geomatics World*, vol. 20, no. 6, pp. 18–20, Sep. 2012.
- [9] D. Laurichesse and F. Mercier, "Integer Ambiguity Resolution on Undifferenced GPS Phase Measurements and Its Application to PPP." Proceedings of the 20th International Technical Meeting of the Satellite Division, Institute of Navigatio. Fort Worth, TX, USA., 2007.
- [10] L. Mervart, Z. Lukes, C. Rocken, and T. Iwabuchi, "Precise Point Positioning with Ambiguity Resolution in Real-Time," in *Proceedings of ION GNSS 2008*, Savannah, GA, USA, Sep. 2008, pp. 397–405.
- [11] P. Collins, F. Lahaye, P. Héroux, and S. Bisnath, "Precise Point Positioning with Ambiguity Resolution using the Decoupled Clock Model," in *Proceedings of ION GNSS 2008*, Savannah, GA, USA, Sep. 2008, pp. 1315–1322.
- [12] M. Ge, M. Gendt, M. Rothacher, C. Shi, and J. Liu, "Resolution of GPS Carrier-Phase Ambiguities in Precise Point Positioning (PPP) with Daily Observations." *Journal of Geodesy*, vol. 82, pp. 389–399, 2008.
- [13] J. Juan, M. Hernández-Pajares, J. Sanz, P. Ramos-Bosch, A. Aragon-Angel, R. Orus, W. Ochieng, S. Feng, P. Coutinho, J. Samson, and M. Tossaint, "Enhanced Precise Point Positioning for GNSS Users." *IEEE Transactions on Geoscience and Remote Sensing* 10.1109/TGRS.2012.2189888, 2012.
- [14] M. Hernández-Pajares, J. Juan, J. Sanz, J. Samson, and M. Tossaint, "Method, Apparatus and System for Determining a Position of an Object Having a Global Navigation Satellite System Receiver by Processing Undifferenced Data Like Carrier Phase Measurements and External Products Like Ionosphere Data. international patent application PCT/EP2011/001512 (ESA ref.: ESA/PAT/566)." 2011.
- [15] T. Yunck, "Coping with the atmosphere and ionosphere in precise satellite and ground positioning." *Environmental Effects on Spacecraft Trajectories and Positioning*, Geophysical Monograph Series, Edited by A. Valance Jones. AGU. Washington, DC, USA., vol. 73, 1993.
- [16] IGS Products, "<http://www.igs.org/products/data>," Jan. 2014.
- [17] O. Colombo, "Real-Time, Wide-Area, Precise Kinematic Positioning Using Data from Internet NTRIP Streams," in *Proceedings of ION GNSS 2008*, Savannah, GA, USA, Sep. 2008, pp. 1315–1322.
- [18] IGS Real Time Pilot Project, "<http://www.rtgis.net>," Jan. 2014.
- [19] A. J. Mannucci, B. D. Wilson, D. N. Yuan, C. H. Ho, U. J. Lindqwister, and T. F. Runge, "A global mapping technique for gps-derived ionospheric total electron content measurements," *Radio Science*, vol. 33, no. 3, pp. 565–582, 1998. [Online]. Available: <http://dx.doi.org/10.1029/97RS02707>
- [20] J. Juan, A. Rius, M. Hernández-Pajares, and J. Sanz, "A two-layer model of the ionosphere using global positioning system data," *Geophysical Research Letters*, vol. 24, no. 4, pp. 393–396, 1997.
- [21] S. Schaer, W. Gurtner, and J. Feltens, "IONEX: The IONosphere Map Exchange Format Version 1," in *Proceeding of the IGS AC Workshop*, Darmstadt, Germany, Feb. 1998, pp. 233–247.
- [22] J. Klobuchar, "Ionospheric Time-Delay Algorithms for Single-Frequency GPS Users." *IEEE Transactions on Aerospace and Electronic Systems*, vol. AES-23, no. 3, pp. 325–331, 1987.
- [23] G. Di Giovanni and S. Radicella, "An Analytical Model of the Electron Density Profile in the Ionosphere." *Advances in Space Research*, vol. 10, no. 11, pp. 27–30, 1990.
- [24] P. J. G. Teunissen, "The geometry-free gps ambiguity search space with a weighted ionosphere," *Journal of Geodesy*, vol. 71, no. 6, pp. 370–383, 1997. [Online]. Available: <http://dx.doi.org/10.1007/s001900050105>

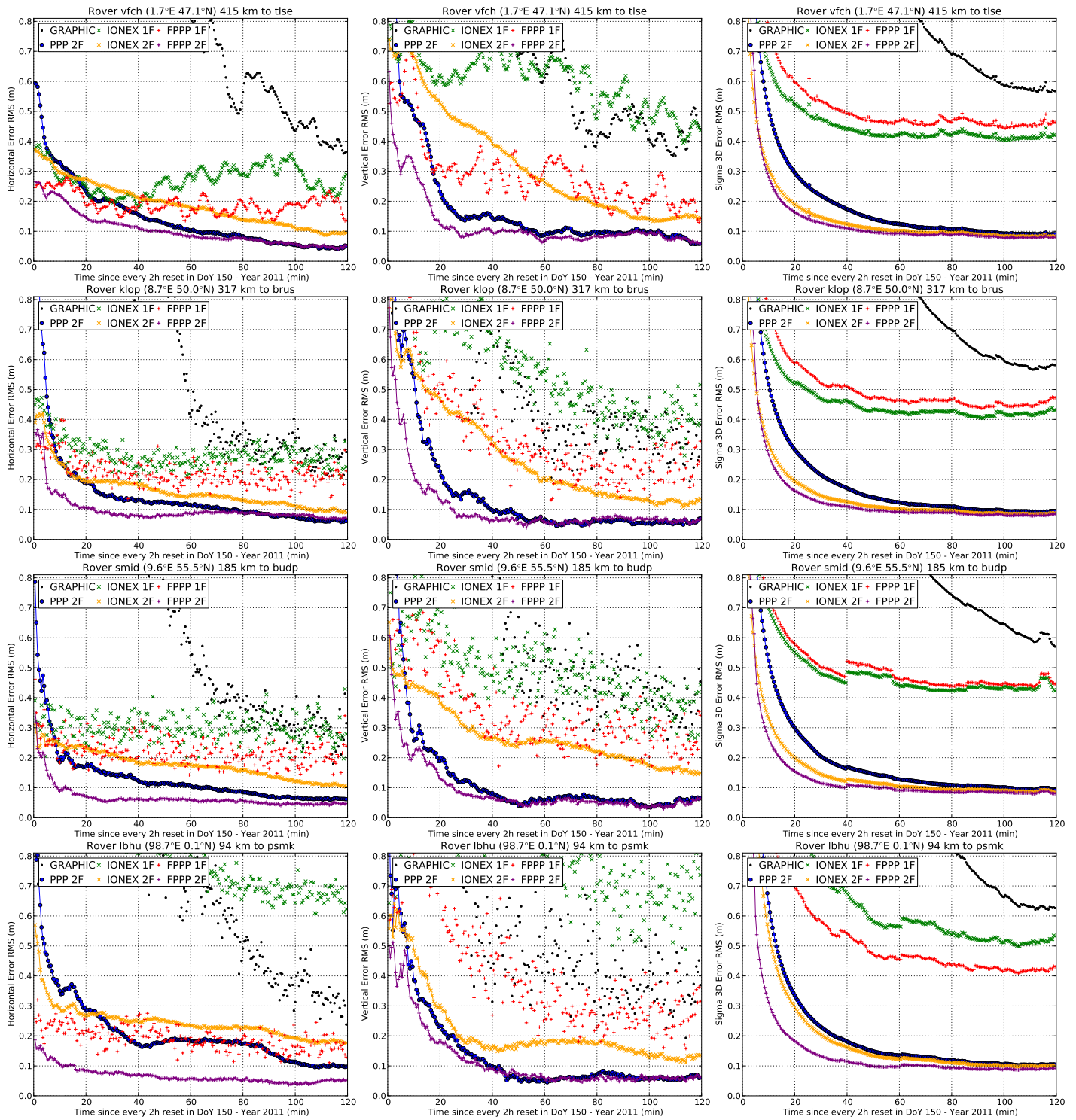


Fig. 6. Convergence assessment: horizontal (left) and vertical (centre) RMS accuracies as a function of time since the user receiver is reset (with resets every 2 hours and 12 resets merged per plot). The right column shows the formal error in 3D position. In each plot, the ionosphere-free solutions for single- and dual-frequency solutions (GRAPHIC and Classic PPP) are compared with the enhanced positioning using ionosphere data from the Fast-PPP and IGS GIMs. The color code used is: GRAPHIC (black), Classic PPP (blue), Fast-PPP single- and dual-frequency (red and pink), IGS-GIMs in IONEX format single- and dual-frequency (green and yellow).

- [25] A. Rovira-Garcia, M. Hernández-Pajares, M. Juan, and J. Sanz, "Fast Precise Point Positioning performance based on International GNSS Real-Time Service data," in *Proceedings of NAVITEC 2012*, ESA/ESTEC, Noordwijk, The Netherlands, Dec. 2012, pp. 1–5.
- [26] S. Datta-Barua, T. Walter, E. Altshuler, J. Blanch, and P. Enge, "Dst as an Indicator of Potential Threats to WAAS Integrity and Availability," in *Proceedings of ION GPS 2005*, USA, Sep. 2005, pp. 2365–2373.
- [27] J. Sanz, J. Juan, G. González-Casado, R. Prieto-Cerdeira, S. S., and R. Orús, "Novel Ionospheric Activity Indicator Specifically Tailored for GNSS Users," in *Proceedings of ION GNSS+ 2014*, Tampa, Florida (USA), Sep. 2014, pp. 1173–1182.
- [28] RTCA-MOPS, "Minimum Operational Performance Standards for Global Positioning System/Wide Area Augmentation System Airborne Equipment.rtc document 229-C," Washington, USA, 2006.

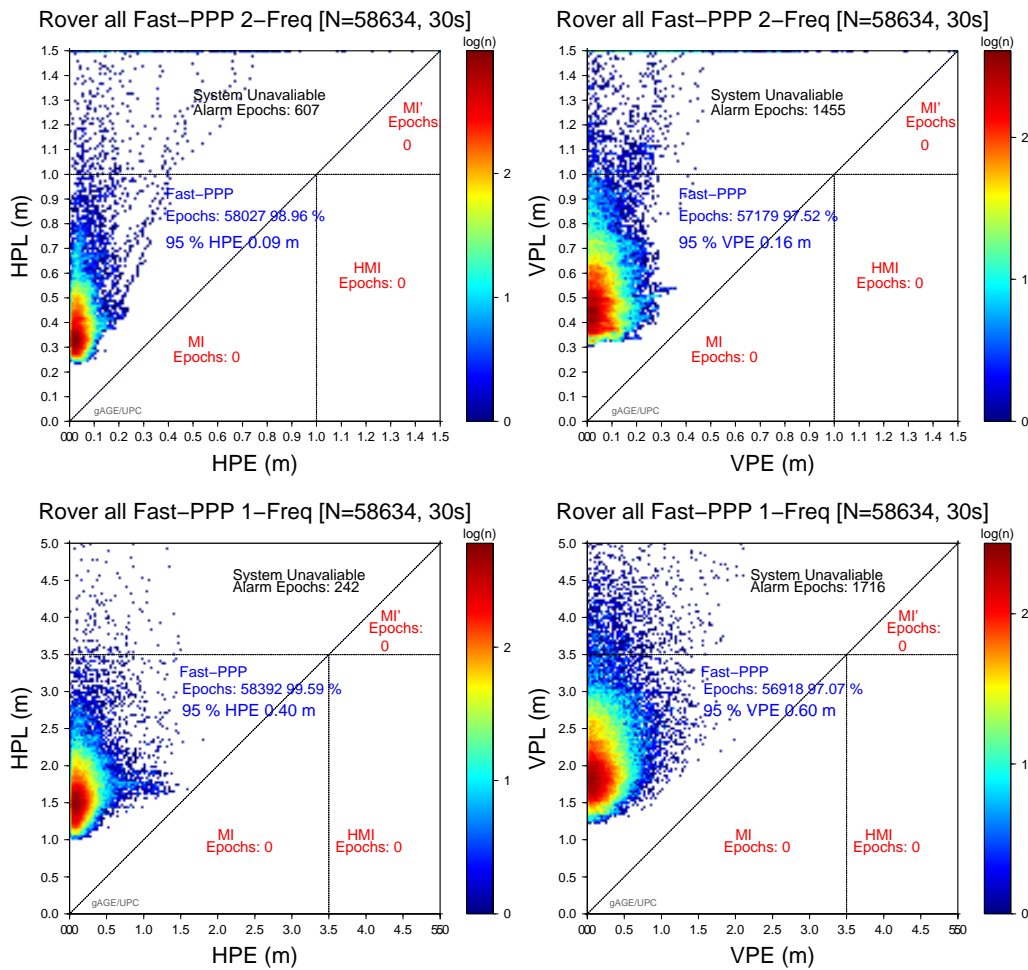


Fig. 7. Fast-PPP Protection Level assessment: horizontal (left) and vertical (right) Stanford plots for dual-frequency (top) and single-frequency (bottom) navigation solutions. Horizontal and Vertical Positioning Errors (HPE and VPE) are bounded by the corresponding Vertical and Horizontal Protection Levels (VPL and HPL). Each plot shows a total of 58634 epochs, merging the computations for the 21 rovers of the 24 hours scenario: DoY 150 of Year 2011, with a sampling rate of 30 seconds. The system is available when the protection level is under 1.0 m (dual-frequency) or 3.5 m (single-frequency).



Adrià Rovira-Garcia received his Aerospace Engineering degree in March 2010 from the Technical University of Catalonia (UPC), Spain. He is currently pursuing a PhD in the Aerospace Science and Technology Aerospace Doctoral Program of UPC. In January 2012, the European Space Agency granted Adrià a PhD. co-sponsorship fellowship together with the industrial partner FUGRO. Since then Adrià's research is focussed in enhanced algorithms related with the real-time Fast-PPP technique.



Dr. Jaume Sanz is teaching at the Technical University of Catalonia (UPC) in Barcelona, Spain, in the Department of Applied Mathematics IV since 1983. They were granted tenure and promoted to Associate Professor in 1988. He obtained the National accreditation for Full Professor in 2011.

He has published over 70 papers in peer-reviewed journals and more than 150 works in meeting proceedings, with 4 best paper awards from the US Institute of Navigation. He co-authors of 5 patents on GNSS and 4 books on GNSS Data Processing.



Dr. José Miguel Juan is teaching at the Technical University of Catalonia (UPC) in Barcelona, Spain, in the Department of Applied Physics since 1988. He was granted tenure and promoted to Associate Professor in 1991. He obtained the National accreditation for Full Professor in 2011.

He has published over 70 papers in peer-reviewed journals and more than 150 works in meeting proceedings, with 4 best paper awards from the US Institute of Navigation. He co-authors of 5 patents on GNSS and 4 books on GNSS Data Processing.



Dr. Guillermo González-Casado is teaching in the Technical University of Catalonia (UPC) in Barcelona, in the Department of Applied Mathematics II, being granted tenure and promoted to Associate Professor in 1999. His current research interests are focused in ionospheric modeling based in GNSS observations and radio occultations, Ground Based Augmentation Systems, and the study and development of GNSS applications in general. He has published about 20 papers in peer-reviewed journals and more than 25 works in meeting proceedings.